2018

Synthesis and Mixing of Complex Halide Perovskites by Solvent-Free Solid-State Methods

Bryan A. Rosales
Iowa State University, brosales@iastate.edu

Lin Wei
Iowa State University, lwei@iastate.edu

Javier Vela
Iowa State University and Ames Laboratory, vela@iastate.edu

Synthesis and Mixing of Complex Halide Perovskites by Solvent-Free Solid-State Methods

Abstract
Halide perovskites are exciting photoactive semiconductors with exceptional photovoltaic and optoelectronic properties. Literature in this area focuses on solution phase aspects of these materials, for example in inks for solar cells, or the growth of bulk or nanosized crystals. Critically, varying solute-solvent interactions often cause heavily mixed perovskites to have compositions that strongly deviate from their synthetic loading. In contrast, hybrid halide perovskites prepared by solid-state methods in the absence of solvents display much more predictable compositions and significantly suppressed phase segregation. Further, because they generate less waste, solvent-free methods are often 'greener' and more industrially scalable. Herein, we review the solvent-free methods used to synthesize single composition 'parent' and heavily mixed perovskites in the solid-state. We discuss the known mechanisms for ion diffusion involved in these transformations, summarize and contrast their main benefits and features, and review their use in the preparation of mixed-cation and/or mixed-halide perovskites.

Keywords
Hybrid halide perovskite, mixed perovskite, solvent-free synthesis, ball milling, thermal annealing

Disciplines
Materials Chemistry

Comments
This is a manuscript of an article published as Rosales, Bryan A., Lin Wei, and Javier Vela. "Synthesis and Mixing of Complex Halide Perovskites by Solvent-Free Solid-State Methods." *Journal of Solid State Chemistry* (2018). doi: 10.1016/j.jssc.2018.12.054. Posted with permission.

Synthesis and Mixing of Complex Halide Perovskites by Solvent-Free Solid-State Methods

Bryan A. Rosales, Lin Wei, Javier Vela

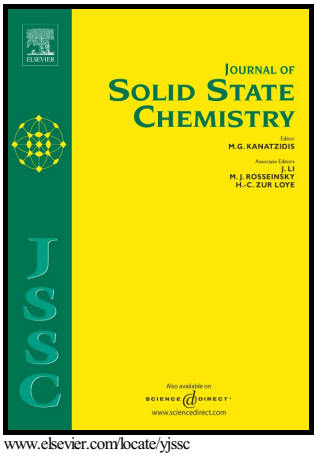

www.elsevier.com/locate/yjssc

PII: S0022-4596(18)30596-6
DOI: https://doi.org/10.1016/j.jssc.2018.12.054
Reference: YJSSC20555

To appear in: *Journal of Solid State Chemistry*

Received date: 17 September 2018
Revised date: 18 December 2018
Accepted date: 27 December 2018

Cite this article as: Bryan A. Rosales, Lin Wei and Javier Vela, Synthesis and Mixing of Complex Halide Perovskites by Solvent-Free Solid-State Methods, *Journal of Solid State Chemistry,* https://doi.org/10.1016/j.jssc.2018.12.054

Synthesis and Mixing of Complex Halide Perovskites by Solvent-Free Solid-State Methods

Bryan A. Rosales[1], Lin Wei[1], Javier Vela[1,2*]

[1]Department of Chemistry, Iowa State University, Ames, Iowa 50011, United States

[2]Ames Laboratory, Iowa State University, Ames, Iowa 50011, United States

* Corresponding author. vela@iastate.edu

Abstract

Halide perovskites are exciting photoactive semiconductors with exceptional photovoltaic and optoelectronic properties. Literature in this area focuses on solution phase aspects of these materials, for example in inks for solar cells, or the growth of bulk or nanosized crystals. Critically, varying solute-solvent interactions often cause heavily mixed perovskites to have compositions that strongly deviate from their synthetic loading. In contrast, hybrid halide perovskites prepared by solid-state methods in the absence of solvents display much more predictable compositions and significantly suppressed phase segregation. Further, because they generate less waste, solvent-free methods are often 'greener' and more industrially scalable. Herein, we review the solvent-free methods used to synthesize single composition 'parent' and heavily mixed perovskites in the solid-state. We discuss the known mechanisms for ion diffusion involved in these transformations, summarize and contrast their main benefits and features, and review their use in the preparation of mixed-cation and/or mixed-halide perovskites.

Graphical Abstract

Solvent-free methods including ball milling and thermal annealing enable the synthesis of heavily mixed halide perovskites with increased phase purity.

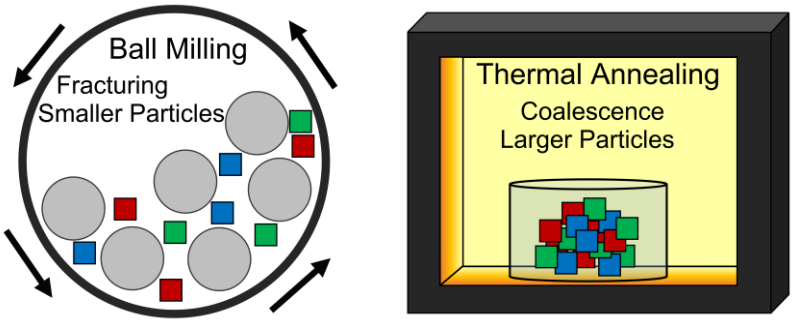

fx1

Keywords

Hybrid halide perovskite, mixed perovskite, solvent-free synthesis, ball milling, thermal annealing.

Acronyms.

MA methylammonium ($CH_3NH_3^+$)

FA formamidinium ($CH(NH_2)_2^+$)

GUA guanidinium ($C(NH_2)_3^+$)

EA ethylammonium ($CH_3CH_2NH_3^+$)

MBA 4-methylbenzylammonium ($CH_3C_6H_4CH_2NH_3^+$)

PEA phenethylammonium ($C_6H_5(CH_2)_2NH_3^+$)

BTA *n*-butylammonium ($CH_3(CH_2)_3NH_3^+$)

DDA *n*-dodecylammonium ($CH_3(CH_2)_{11}NH_3^+$)

ODA *n*-octadecylammonium ($CH_3(CH_2)_{17}NH_3^+$)

NMA 1-naphthylmethylammonium ($C_{10}H_7CH_2NH_3^+$)

1. Introduction.

Halide perovskites of the general formula ABX_3—where A = methylammonium ($CH_3NH_3^+$ or 'MA'), formamidinium ($CH(NH_2)_2^+$ or 'FA'), guanidinium ($C(NH_2)_3^+$ or 'GUA'), Cs^+, Rb^+, K^+; B = Pb^{2+}, Sn^{2+}, Ge^{2+}; and X = I^-, Br^-, Cl^-—are an emerging class of semiconductors that have revolutionized the field of light-harvesting materials. In less than a decade of research,[1] thin film perovskite solar cells reached 23.7% power conversion efficiency (PCE),[2] while perovskite-based quantum dot solar cells reached a record 15.07% PCE.[3] Perovskite solar cell materials are mostly comprised of earth abundant elements and are easily processed from solution, which makes them compatible with roll-to-roll and other high-volume thin film

manufacturing techniques.[4] Halide perovskites are also excellent photonic sources by exhibiting efficient radiative recombination (>50%) under high excitation densities, large and balanced charge-carrier mobilities, high free-carrier densities, and large gain coefficients.[5] In addition, the large degree of chemical and structural diversity in halide perovskites results in many unique properties such as band gap tunability over the visible and near-infrared spectrum, large absorption coefficients, long carrier recombination, defect tolerance, photon recycling, magnetism, ferroelectricity, ferroelasticity, and multiferroicity.[6,7]

Many of the best performing halide perovskite solar cells are made of 'mixed' materials comprised of a mixture of cations and/or anions.[8,9] Typically, the adjective hybrid refers only to halide perovskites that contain both organic (MA, FA, GUA, etc.) and inorganic (Pb, Sn, Ge) ions. In contrast, the adjective all-inorganic refers to halide perovskites that contain only inorganic (Cs, Rb, K, ect.; Pb, Sn, Ge) ions. Here, we review all mixed-cation and mixed-anion halide perovskites under the same umbrella, regardless of whether these are hybrid or all-inorganic.

To date, much of the perovskite literature has focused on their synthesis from solution, for example as inks for solar cells,[10] the growth of single crystals,[10] or the preparation of colloidal nanocrystals.[11,12] When heavily mixed perovskites are prepared from solution, solute-solvent interactions can vary for each different precursor component.[13] As a result, solute-solvent interactions can alter the composition of the final product(s).[14,15,16,17,18,19,20] In contrast, the synthesis of heavily mixed perovskites by solvent-free or 'solventless' methods circumvents the effects of these different binding affinities and other solute-solvent interactions. As a result, heavily mixed halide perovskites prepared in the solid-state by solvent-free methods show suppressed phase segregation compared to their solution phase counterparts.[14,15,16,17] Further, solvent-free methods are generally considered 'greener' because they generate less waste;[21] they are also often more industrially scalable.[21]

Here, we review various solvent-free solid-state methods used to synthesize single composition and heavily mixed halide perovskites. We start with a discussion on ion migration and transport in halide perovskites to better understand the mechanisms of solid-state ion diffusion. We continue with a discussion on the thermal properties and decomposition pathways of halide perovskites. Next, we summarize the different solvent-free synthesis methods employed to prepare 3D, 2D, double, and defect halide perovskites, including their underlying

physical processes, comparative benefits, and differences. Lastly, we review current research on mixed-halide perovskites, mixed-cation perovskites, and perovskites that contain both mixed-cations and mixed-halides. It is our hope that this review will stimulate sustained high-level research that will further increase our understanding of solvent-free, solid-state synthesis of heavily mixed halide perovskites and other advanced semiconductors.

2. Ion Transport in Halide Perovskites.

Ion transport is known to readily occur in oxide- and halide-based perovskites. Here, we highlight mechanisms of ion transport in halide perovskites; those in chalcogenide perovskites appear elsewhere.[22,23] Halide perovskites crystallize easily, which leads to inexpensive processing at low temperatures.[10] This distinctive property leads to a soft and dynamic lattice in which ions readily move around. Halide perovskites are excellent ionic conductors. As a consequence, ion exchange in these materials occurs easily and rapidly,[12,24] serving as useful solid electrolytes.[25] This large degree of ion mobility is responsible for many unusual properties, including rapid chemical conversion between halides at room temperature, current-voltage hysteresis, above band-gap photovoltages, light-induced lattice expansion and phase separation, and self-healing.[26,27,28]

Ion transport in halide perovskites is believed to be mediated by point defects.[26,27,28] Figure 1 shows various mechanisms of ion transport that are known in these materials, including A-, B-, and X-site vacancy diffusion and X-interstitial diffusion. In each case, the respective ionic species hops to the nearest neighboring vacancy or interstitial site.[26] Because diffusion of ions requires energy, the dominant ion transport mechanism is determined by both its activation energy and the concentration of lattice defects.[26,27,28] A large range of activation energies are reported in the literature. For example, in the case of $MAPbI_3$, the lowest activation energy for ion migration is 0.1–0.6 eV for I^- vacancies, followed by 0.5–0.8 eV for $CH_3NH_3^+$ vacancies, and 0.8–2.3 eV for Pb^{2+} vacancies.[29] These activation energy values suggest that ion transport follows the trend $I^- > CH_3NH_3^+ > Pb^{2+}$. Indeed, the most mobile ions in perovskites are halides, exchanging in a matter of seconds; in contrast, cations are less mobile, exchanging over a few hours.[26] Even though halide mobility under illumination is well established, it was recently shown that $CH_3NH_3^+$ diffusion is negligible under illumination.[30] Ion transport in halide perovskites is enhanced by a variety of external stimuli, which can be optical, electrical, thermal,

chemical, or mechanical in nature.[26] Interestingly, ion transport can also be structurally modulated; for example, mixed-cation halide perovskites are able to suppress photo-induced halide segregation.[31,32]

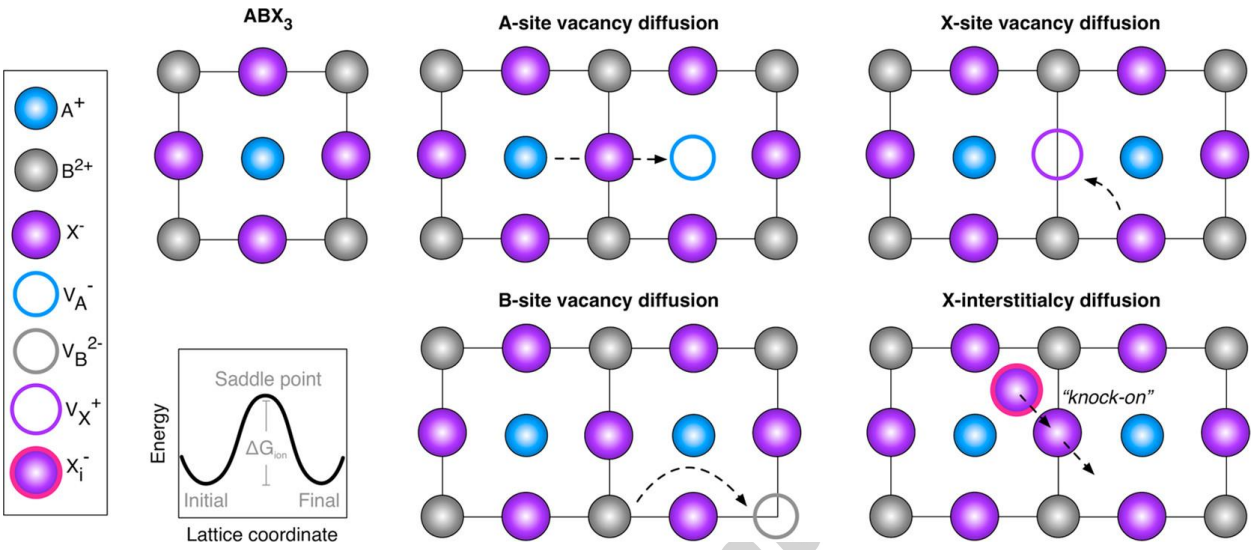

Figure 1. Mechanisms of ion transport in halide perovskites. Filled circles represent regular lattice sites containing ions, empty circles represent vacancies, and the pink halo denotes an interstitial halide. Reprinted with permission from ref. 26. Copyright 2018 American Chemical Society.

3. Thermal Properties of Halide Perovskites.

Synthesis by solvent-free methods often requires high temperatures. Thus, information about the melting points and decomposition temperatures of a material is imperative when planning a solid-state reaction. Table 1 provides a summary of the known melting points and decomposition temperatures of commonly used single-composition or 'parent' halide perovskites. All-inorganic halide perovskites melt congruently without decomposition, at temperatures ranging from 475–615 °C for $CsPbX_3$,[33,34,35,36,37] and 368–452 °C for $CsSnX_3$.[38,39] In contrast, hybrid halide perovskites decompose before melting at temperatures ranging from 214–300 °C for $MAPbX_3$,[40,41,42] 150–300 °C for $MASnX_3$,[40,43] and 250–320 °C for $FABX_3$ (B = Pb, Sn).[40,44,45,46] TGA-DTA/MS measurements show that $MAPbI_3$ decomposes into solid PbI_2, along with the evolution of gaseous NH_3 and CH_3I.[47] Decomposition of other $MAPbX_3$ perovskites can produce gaseous CH_3NH_2 and HX. Similarly, TGA-DSC measurements show that thermal

decomposition of $FAPbI_3$ starts by loss of HI.[44] The decomposition temperature of Sn-based halide perovskites is believed to depend on the concentration of Sn(IV) species generated from oxygen exposure; it is 300 °C under inert atmosphere and decreases to 150 °C upon exposure to air.[40] In summary, to prevent the formation of undesired impurities and off-stoichiometric products, the solid-state synthesis of hybrid halide perovskites must be conducted below their decomposition temperature.

Table 1. Thermal Properties of Halide Perovskites

Composition	mp[a] (°C)	T_{dec}[b] (°C)
$CsPbI_3$	475[33]	-
$CsPbBr_3$	500[34], 567[35,36]	-
$CsPbCl_3$	600[34], 615[37]	-
$CsSnI_3$	435[38], 452[39]	-
$CsSnBr_3$	448[39]	-
$CsSnCl_3$	368[39]	-
$MAPbI_3$	-	240[42], 300[40,41]
$MAPbBr_3$	-	260[42]
$MAPbCl_3$	-	214[42], 260[41]
$MASnI_3$	-	150-300[40]
$MASnBr_3$	-	175[43]
$MASnCl_3$	-	-
$FAPbI_3$	-	250[40], 300[44], 320[44]
$FAPbBr_3$	-	280[46]
$FAPbCl_3$	-	-
$FASnI_3$	-	280[40]
$FASnBr_3$	-	-
$FASnCl_3$	-	-

[a]mp = melting point, [b]T_{dec} = decomposition temperature.

4. Solvent-Free Synthesis: Methods and Parent Halide Perovskites.

Solid-state methods for the preparation of single-composition or 'parent' halide perovskites in the absence of solvents include mechanochemistry (ball milling or manual grinding) and thermal annealing. Now over 120 years old,[48] mechanochemistry has undergone a resurgence as an industrially-scalable 'green' chemistry method due to its relatively mild operation conditions and its independence from solvents.[21] The energy for ball milling is supplied by rotation of the sample's containment bowl (see Figure 2). The bowl and a set of grinding balls are typically made of a high-hardness material (zirconia, corundum, or stainless steel), such that when precursors are crushed between the balls, mechanical energy is transferred from the balls to the precursors. This leads to elastic and plastic deformation, and finally fracturing to produce dislocations that react together to form the product.[49,50] Optimization of various parameters such as bowl rotation speed and number of grinding balls controls the amount of mechanical energy applied to the system and the size of the crystallites that are produced. Because these parameters are responsible for the total energy input provided to the system, care must be taken to consider the amount of heat that develops internally and, thus, the actual

reaction temperature of the reaction. Because the internal temperature is not always monitored, mechanical grinding and thermal annealing combined may be, in some cases, responsible for driving a ball milling reaction, thus affecting its specific synthetic outcome. In other words, ball milling reactions cannot always be safely assumed to proceed at room temperature, unless the temperature inside the ball mill is being actively monitored. Additionally, while ball milling has many benefits, contamination can occur due to wearing of the bowl and grinding balls (*e.g.*, iron from steel balls, which typically exists at concentrations below the relative detection limit of XRD).[21]

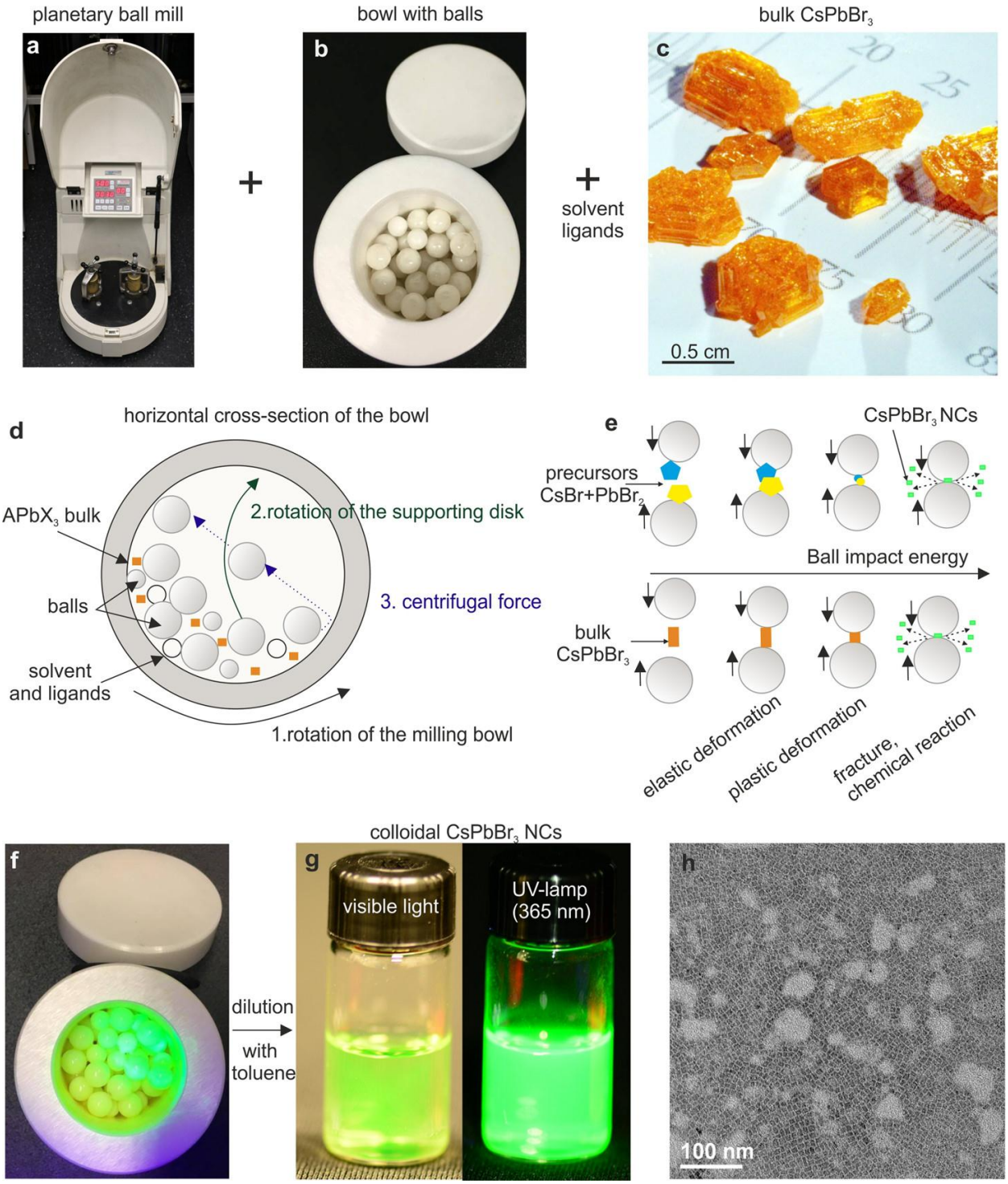

Figure 2. Typical ball mill (a), zirconia bowl and balls (b), and precursor crystals (c). Cross-section of a ball mill under operation (d). Processes that initiate a mechanochemical reaction (e). Perovskite nanocrystals treated with surface ligands after ball milling and (f) upon dilution with toluene (g). TEM image of perovskite nanocrystals prepared by ball milling (h). Reprinted with

permission from ref. 50, https://pubs.acs.org/doi/10.1021/acsanm.8b00038. Further permissions related to the material excerpted should be directed to the ACS.

Mechanochemical synthesis at room temperature is particularly ideal for the solid-state synthesis of hybrid halide perovskites given their inherently low thermal stability[51] and high vapor pressure of organic cation salts, when present. Hybrid halide perovskites synthesized by mechanochemistry are typically made by either ball milling[52,53,54,55,56] or manual grinding[40,57] a mixture of solid AX and BX_2 precursors at room temperature, without the addition of solvents (Scheme 1a). While manual grinding often leaves small amounts of unreacted precursors,[40,57] ball milling typically results in cleaner crystalline products by X-ray diffraction (XRD).[52,54,56] In addition to 3D perovskites, a variety of 0D, 1D, and 2D perovskite analogues can be made by mechanochemical synthesis, for example by using bulky organic cations or by changing the stoichiometry of the precursors.[58,59,60,61,62,63] Luminescent perovskite nanocrystals are easily produced due to the reduction of crystallite size that is inherent to ball milling, as demonstrated under completely dry,[55,57,58] wet,[50, 64] or after post-milling oleylamine-treatment conditions (Figure 2).[65] In fact, ball milling can generate luminescent perovskite nanocrystals through size reduction of bulk perovskite powders (Figure 2).[50] Hybrid halide perovskites prepared by mechanochemistry display beneficial properties including stability at higher temperatures[52] and reduction of interfacial trap density.[54] Mechanochemistry also allows for doping of insoluble additives that can enhance photovoltaic properties.[66]

Scheme 1. Synthesis of 3D, 2D, Double, and Defect Halide Perovskites.

(a) $AX + BX_2 \rightarrow ABX_3$

(b) $AX + A'X' + BX_2 + BX'_2 \rightarrow (A,A')B(X,X')_3$

(c) $ABX_3 + ABX'_3 \rightarrow AB(X,X')_3$

(d) $ABX_3 + A'BX_3 \rightarrow (A,A')BX_3$

(e) $ABX_3 + AB'X_3 \rightarrow A(B,B')X_3$

(f) $ABX_3 + A'BX'_3 \rightarrow (A,A')B(X,X')_3$

(g) $2\,AX + (n\text{-}1)\,A'X + n\,BX_2 \rightarrow A_2A'_{n-1}B_nX_{3n+1}$

(h) $2\,AX + A'X + PnX_3 \rightarrow A_2A'PnX_6$

(i) $3\,AX + 2\,PnX_3 \rightarrow A_3Pn_2X_9$

(j) $3\,A + 2\,Pn + 9/2\,X_2 \rightarrow A_3Pn_2X_9$ (elemental precursors)

A, A′ = methylammonium ($CH_3NH_3^+$, MA), formamidinium ($CH(NH_2)_2^+$, FA), guanidinium ($C(NH_2)_3^+$, GUA), alkylammonium ($CH_3(CH_2)_xNH_3^+$), Cs^+, Rb^+, K^+, Ag^+

B, B′ = Pb^{2+}, Sn^{2+}, Ge^{2+}

X, X′ = I^-, Br^-, or Cl^-

Pn = Bi^{3+} or Sb^{3+}

In contrast to mechanochemistry, synthesis by thermal annealing is diffusion-limited. The success of thermal annealing depends on reactive species being able to diffuse through the bulk of the material to the interface between the reacting solids.[67] As the precursor solids interact with each other, coarsening occurs, resulting in increased crystallite sizes (*i.e.*, the opposite to nanostructuring often observed after ball milling). Precursors are typically ground together and may be packed into a pellet to reduce the path for mass diffusion. Solid-state synthesis by thermal annealing can be performed in an ampule sealed under vacuum or under an inert gas, if air sensitive reagents are used. Because of its Arrhenius-like behavior, high-temperatures are sometimes necessary to overcome the activation energy for mass diffusion or to increase its rate.[67]

The limited thermal stability range of hybrid halide perovskites, high organic cation precursor vapor pressure, and the inherent need for higher temperatures can render the direct solid-state synthesis of hybrid 3D halide perovskites by thermal annealing somewhat challenging. In contrast, all-inorganic 3D halide perovskites are easily made by thermally annealing a mixture of CsX and BX_2 (M = Pb, Sn) precursors in an sealed evacuated ampule between 200–600 °C for

several hours (Scheme 1a).[38,40,68,69,70,71,72] A variety of Ruddlesden-Popper hybrid 2D halide perovskites[73] of the general formula $A_2A'_{n-1}B_nX_{3n+1}$ (A,A' = Cs, ethylammonium ($CH_3CH_2NH_3^+$ or 'EA'), 4-methylbenzylammonium ($CH_3C_6H_4CH_2NH_3^+$ or MBA), phenethylammonium ($C_6H_5(CH_2)_2NH_3^+$ or PEA), *n*-butylammonium ($CH_3(CH_2)_3NH_3^+$ or BTA); B = Pb, Sn; X = I, Br, Cl) can be made by thermally annealing a mixture of AX and BX_2 precursors in a ratio corresponding to the desired *n* level in an ampule between 80–500 °C for several hours (Scheme 1g).[74,75,76,77] Double perovskites of the general formula $A_2A'PnX_6$ (A,A' = MA, Cs, Ag; Pn = Bi, Sb; X = I, Br, Cl) are commonly made by thermally annealing a mixture of AX and PnX_3 precursors between 210–500 °C for several hours (Scheme 1h).[78,79,80,81,82] Defect perovskites of the general formula $A_3Pn_2I_9$ (A = Cs, Rb, Tl; Pn = Bi, Sb) can also be made by thermally annealing a mixture of AI and PnI_3 precursors between 650-1130 °C for several hours (Scheme 1i)[83,84,85,86] or a mixture of elemental Tl, Bi, and I_2 in a sealed evacuated ampule at 530 °C (Scheme 1j).[87] Solid-state synthesis of mixed-halide and mixed-cation halide perovskites by thermal annealing is successful when starting from a mixture of two pre-synthesized, single-composition perovskites between 150–200 °C.[14,15,72]

Thermal annealing can be used for thin film fabrication through melt processing. Melt-processing typically involves heating pre-formed perovskite[88,89,90,91,92] or a mixture of AX + BX_2 precursors[75] deposited onto a substrate above their melting point by pressing downward with another heated substrate, typically polyimide or glass.[93] Melt-processing is particularly useful for thin film growth because of its ability to avoid pinholes and voids that are commonly observed by conventional solution crystallization.[93] Because of the high melting points (400–600 °C, see section 3) of all-inorganic $CsBX_3$ perovskites (B = Pb, Sn) and low decomposition temperatures (150–300 °C, see section 3) of hybrid ABX_3 perovskites (A = MA, FA; B = Pb, Sn; X = I, Br, Cl), melt-processing has not been employed for 3D halide perovskites. In contrast, melt-processing is used for hybrid 2D halide perovskites because their melting points can be lowered below decomposition [93] (for example, by increasing the bulkiness of the organic cation, which results in melting points tunable over a 100 °C window).[88,89] Table 2 summarizes various reports of solvent-free solid-state synthesis of halide perovskites.

Table 2. Solid-State Synthesis of 3D, 2D, Double, and Defect Halide Perovskites by Solvent-Free Methods.

Precursors[a]	**Methods**	**Conditions**	**Products[a]**	**Refs.**
$CH_3NH_3I + PbI_2$	Ball milling	10 mm balls, 30 Hz, 30 min	$MAPbI_3$	52,54
$CH_3NH_3I + PbI_2$	Ball milling	3 mm balls, 200-600 rpm	$MAPbI_3$	53

$CH_3NH_3X + PbX_2$ (X = I, Br)	Ball milling	10 mm balls, 300 rpm, 40 min	$MAPb(I,Br)_3$	56
AI + PbI_2 (A = MA, FA, GUA)	Ball milling	10 mm balls, 350 rpm, 10 min	$MAPbI_3$, $FAPbI_3$, GUA_2PbI_4	61
CsI + PbI_2	Ball milling	10 mm balls, 25 Hz, 30 min	$CsPbI_3$	102
CsBr + $PbBr_2$	Ball milling	10 mm balls, 500 rpm, 4 h	$CsPbBr_3$	55
CsBr + $PbBr_2$	Ball milling	10 mm balls, 25 Hz, 30 min	$CsPbBr_3$	66
CsBr + $PbBr_2$ + oleylNH_3Br[b]	Ball milling[b]	4 or 5 mm balls, 500 rpm, 2 h	$CsPbBr_3$	50
CsCl + $PbCl_2$	Ball milling	10 mm balls, 30 Hz, 30 min	$CsPbCl_3$	66
KI + PbI_2	Ball milling	10 mm balls, 25 Hz, 30 min	$KPbI_3$	102
KI + PbI_2	Ball milling	10 mm balls, 25 Hz, 30 min	KPb_2Br_5	102
$CH_3NH_3X + PbX_2$ (X = I, Br)	Ball milling	10 mm balls, 300 rpm, 40 min	$MAPb(I,Br)_3$	97
$MAPbCl_3 + MAPbBr_3$	Ball milling	1 h	$MAPb(Br,Cl)_3$	16
$FAPbX_3 + FAPbX'_3$ (X, X' = I, Br, Cl)	Ball milling	400 rpm	$FAPb(X,X')_3$ (X, X' = I, Br, Cl)	17
AX + PbI_2 (A = MA, hexylNH_3; X = I, Br, Cl)	Ball milling	10 mm balls, 300 rpm, 1–3 h	$APb(I,X)_3$ (A = MA, $C_6H_{13}NH_3$; X = I, Br, Cl)	58
$CsX + PbX_2$ (X = I, Br, Cl)	Ball milling	10 mm balls, 500 rpm, 30 min	$CsPb(X,X')_3$	65
CsBr +PbI_2	Ball milling	10 mm balls, 25 Hz, 30 min	$CsPb(I_2Br)$	102
$CsX + PbX_2$ (X = Br, Cl)	Ball milling	10 mm balls, 30 Hz, 30 min	$CsPb(Br_{1.5}Cl_{1.5})$	66
KI + PbX_2 (X = I, Br)	Ball milling	10 mm balls, 25 Hz, 30 min	$KPb(I_2Br)$	102
AI + PbI_2 (A = MA, FA)	Ball milling	10 mm balls, 30 Hz, 30 min	$(MA,FA)PbI_3$	98,100
AI + PbI_2 (A = K, Cs, MA, FA)	Ball milling	10 mm balls, 25 Hz, 30 min	$(K,Cs,MA,FA)PbI_3$	102
AI + PbX_2 (A = K, Cs; X = I, Br)	Ball milling	10 mm balls, 25 Hz, 30 min	$(K_{0.075}Cs_{0.925})Pb(I_2Br)$	102
KI + CH_3NH_3Br + $CH(NH_2)_2I$ + PbX_2 (X = I, Br)	Ball milling	10 mm balls, 25 Hz, 30 min	(K,MA,FA)Pb(I,Br)	102
CsI + CH_3NH_3Br + $CH(NH_2)_2I$ + PbX_2 (X = I, Br)	Ball milling	10 mm balls, 30 Hz, 30 min	$Cs_{0.05}(MA_{0.17}FA_{0.83})_{0.95}Pb(I_{0.83}Br_{0.17})_3$	66
CsI + CH_3NH_3Br + $CH(NH_2)_2I$ + PbX_2 (X = I, Br)	Ball milling	3 mm balls, 150 rpm, 16 h	$Cs_{0.05}(MA_{0.17}FA_{0.83})_{0.95}Pb(I_{0.83}Br_{0.17})_3$	103
AI + BI_2 (A = MA, FA; B = Pb, Sn)	Grinding	25 °C	ABI_3 (A = MA, FA; B = Pb, Sn),	40
ABr + $PbBr_2$ (A = Cs, MA, FA)	Grinding	25 °C, 10 min	$APbBr_3$ (A = MA, FA, Cs)	57
ABr + $PbBr_2$ (A = Cs, MA, FA) + octylNH_3Br	Grinding	25 °C, 10 min	$APbBr_3$ (A = MA, FA, Cs)	57
$CsX + PbX_2$ (X = I, Br, Cl)	Grinding	25 °C, 2 h, N_2	$CsPbX_3$, $CsPb_2X_5$, Cs_4PbX_6 (X = I, Br, Cl)	59
$MAPbCl_3 + MAPbBr_3$	Grinding	25 °C, 2 h	$MAPb(Br,Cl)_3$	16
$FAPbX_3 + FAPbX'_3$ (X, X' = I, Br, Cl)	Grinding	25 °C	$FAPb(X,X')_3$ (X, X' = I, Br, Cl)	17
AI + PbI_2 (A = MA, GUA)	Grinding	25 °C, Ar	$(MA,GUA)PbI_3$	101
$CH_3NH_3I + BI_2$ (B = Pb, Sn)	Grinding	25 °C	$MA(Pb,Sn)I_3$	40
$CsPbBr_3$ + KX (X = I, Br, Cl)	Grinding[c]	5 min, 2.2 GPa, N_2	$CsPbX_3$ (X = I, Br, Cl)	95
ABr + $SnBr_2$ (A = BTA, MBA, DDA, ODA, NMA)	Grinding	25 °C	A_2SnBr_4 (A = BTA, MBA, DDA, ODA, NMA)	62
ABr + A'Br + $SnBr_2$ (A = BTA, MBA, DDA, ODA, NMA; A' = Cs, MA)	Grinding	25 °C	$A_2A'Sn_2Br_7$ (A = BTA, MBA, DDA, ODA, NMA; A' = Cs, MA)	62
$CsCl + CuCl_2 \bullet 2H_2O + SbCl_3$	Grinding	25 °C, 10 min	$Cs_4CuSb_2Cl_{12}$	63
AI + BI_2 (A = MA, FA; B = Pb, Sn)	Annealing	200 °C, 2 h, vac.	ABI_3 (A = MA, FA; B = Pb, Sn)	40
AI + BI_2 (A = MA, FA; B = Pb, Sn)	Annealing	350 °C, 1 min, N_2	ABI_3 (A = MA, FA; B = Pb, Sn)	40
CsI + SnI_2	Annealing	550 °C, 1 h, vac.	$CsSnI_3$	38
CsI + SnI_2	Annealing	190-370 °C, N_2	$CsSnI_3$	69
CsI + SnI_2 + SnF_2	Annealing	400 °C, 5 h, vac.	$CsSnI_3$, Cs_2SnI_6	71
CsBr + $PbBr_2$	Annealing	600 °C, 11 h, vac.	$CsPbBr_3$	72
$AX + SnX_2$ (A = Cs, Rb; X = I, Cl)	Annealing	400–750 °C, 8–24 h, N_2	$A_xSn(Cl_yI_z)$ (A = Cs, Rb)	60
$CsX + SnX'_2$ (X, X' = I, Br, Cl)	Annealing	490 °C, 1-2h, vac. or N_2	$CsSn(X,X')_3$ (X, X' = I, Br, Cl)	68
CsI + SnI_2 + SnF_2	Annealing	450 °C, 30 min, vac.	$CsSn(I,F)_3$	70
$MAPbX_3 + MAPbX'_3$ (X, X' = I, Br, Cl)	Annealing	50–250 °C, 1 h	$MAPb(X,X')_3$ (X, X' = I, Br, Cl)	14,15
$CsPbBr_3 + MAPbBr_3$	Annealing	150 °C, 5 d, vac.	$(Cs,MA)PbBr_3$	72
$CH_3NH_3I + BI_2$ (B = Pb, Sn)	Annealing	200 °C, 2 h, vac.	$MA(Pb,Sn)I_3$	40
$CH_3NH_3I + BI_2$ (B = Pb, Sn)	Annealing	350 °C, 1 min, N_2	$MA(Pb,Sn)I_3$	40
ABr + $PnBr_3$ + $PbBr_2$ (A = MA, Cs, Ag; Pn = Bi, Sb)	Annealing	100-320 °C, vac.	$A(Ag/Pn,Pb)Br_3$ (A = Cs, MA; Pn = Bi, Sb)	94
EAX + PbX_2 (X = Br, Cl)	Annealing	80 °C, 2 h	$EA_4Pb_3(Br,Cl)_{10}$	74
AX + BX_2 (A = MBA, PEA, BTA)	Annealing	Melt, hours	A_2BX_4 (A = MBA, PEA, BTA)	75
CsI + $PbCl'_2$ (X,X' = I, Cl)	Annealing	500 °C, 24 h	$Cs_2PbI_2Cl_2$	76
BTAI + EuI_2	Annealing	160 °C, 8 h	BTA_2EuI_4	77
MAI + AgI + SbI_3	Annealing	150 °C, 2 h, vac.	MA_2AgSbI_6	78
CsBr + AgBr + $PnBr_3$ (Pn = Br, Sb)	Annealing	320 °C,20 h, vac.	$Cs_2Ag(Bi,Sb)Br_6$	79
CsBr + AgBr + $BiBr_3$ + MBr_3 (M = Sb, In)	Annealing	320 °C,20 h, vac.	$Cs_2Ag(M,Bi)Br_6$ (M = Sb, In)	80

$CsX + AgX + BiX_3$	Annealing	210 °C, 10 h	Cs_2AgBiX_6 (X = Br, Cl)	81
$CsX + AgX + BiX_3$	Annealing	500 °C, 5 h, vac.	Cs_2AgBiX_6 (X = Br, Cl)	82
$CsI + BiI_3$	Annealing	650 °C, 24 h	$Cs_3Bi_2I_9$	83
$RbI + BiI_3$	Annealing	1130 °C, vac.	$Rb_3Bi_2I_9$	84
$AI + BiI_3$ (A = Cs, Rb)	Annealing	650-700 °C, 10 h, vac.	$A_3Bi_2I_9$ (A = Cs, Rb)	85,86
$Tl + Bi + I_2$	Annealing	530 °C, vac.	$Tl_3Bi_2I_9$	87

[a]MA = methylammonium ($CH_3NH_3^+$), FA = formamidinium ($CH(NH_2)_2^+$), GUA = guanidinium ($C(NH_2)_3^+$), EA = ethylammonium ($CH_3CH_2NH_3^+$), MBA = 4-methylbenzylammonium ($CH_3C_6H_4CH_2NH_3^+$), PEA = phenethylammonium ($C_6H_5(CH_2)_2NH_3^+$), BTA = *n*-butylammonium ($CH_3(CH_2)_3NH_3^+$), DDA = *n*-dodecylammonium ($CH_3(CH_2)_{11}NH_3^+$), ODA = *n*-octadecylammonium ($CH_3(CH_2)_{17}NH_3^+$), NMA = 1-naphthylmethylammonium ($C_{10}H_7CH_2NH_3^+$). [b]Mesitylene and ligands added. [c]Magnetically stirred without a mortar and pestle.

5. Mixed-Halide Perovskites.

Among the earliest reports on the solvent-free synthesis of mixed-halide perovskites was the preparation of all-inorganic Sn-based perovskites from the thermal annealing of CsX and SnX'_2 precursors in a sealed ampule at 400–500 °C for several hours (Scheme 1b).[68] Hybrid mixed-halide Pb-based perovskites were first prepared by the thermal annealing of a mixture of two single-halide perovskites in the desired stoichiometry at 200 °C (Scheme 1c).[14,15] As discussed previously, halide diffusion occurs rapidly in halide perovskites: complete halide exchange occurs immediately in the presence of a KX matrix,[95] and in under an hour between two different single-halide perovskites.[14,15] Figure 3a shows that the two distinct lattice parameters and band gaps that are initially observed in an equimolar mixture of $MAPbI_3$ and $MAPbBr_3$ gradually merge into a single lattice parameter and band gap after annealing at 200 °C for 1 h. Powder XRD shows an initial reduction in the single crystalline (Scherrer) domain size, followed by an increase, which is caused by halide diffusion, exchange and interfacial nucleation, followed by the growth of a new mixed-halide phase, respectively (Figure 3b). Hybrid halide perovskites have limited thermal stability, resulting in their degradation to various PbX_2 byproducts when heated at or above 250 °C. Recently, solid-state halide diffusion in a perovskite heterostructure, made by stacking a $CsPbCl_3$ microplate on top of $CsPbBr_3$ nanowires was optically studied *via* spatially resolved photoluminescence.[96] These measurements, performed at different temperatures, yielded an activation energy of 0.44 ± 0.02 eV for chloride/bromide exchange, and a room-temperature inter-diffusion coefficient of ~10^{-13} cm^2 s^{-1}.[96]

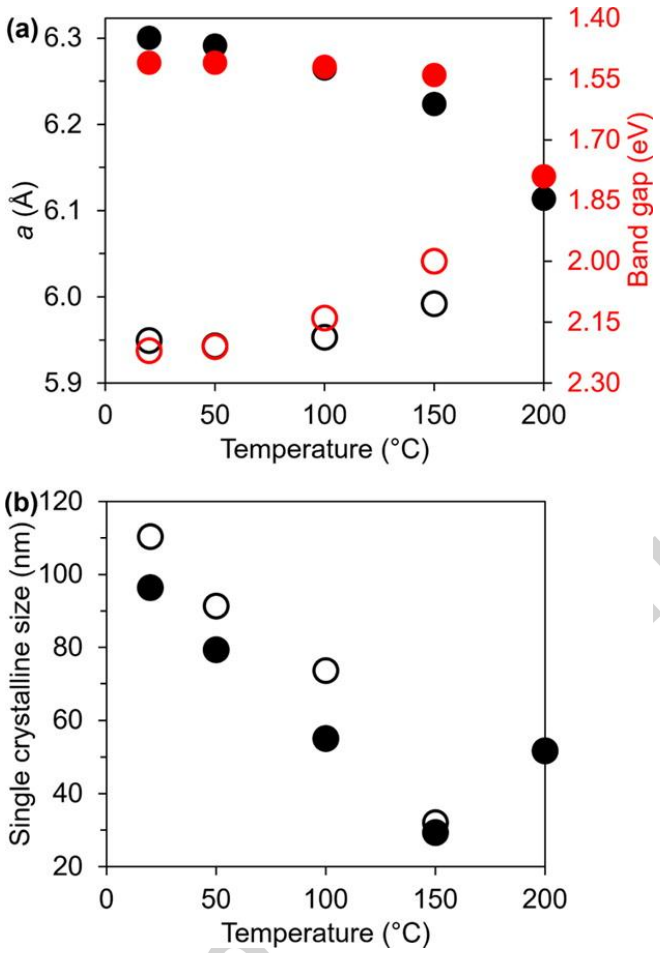

Figure 3. Effect of annealing temperature on an equimolar mixture of $MAPbI_3$ (solid circles) and $MAPbBr_3$ (open circles). Two different lattice parameters and band gaps gradually merge into a single value (a). XRD shows an initial decrease in the single crystalline domain size (interfacial nucleation) followed by a subsequent increase (growth of new phase) (b). Reprinted with permission from ref. 14. Copyright 2016 American Chemical Society.

Mixed-halide perovskites were subsequently synthesized mechanochemically, by either ball milling a mixture of AX and PbX_2 (Scheme 1a)[58,65,97] or by ball milling or manually grinding a mixture of two single-halide perovskites (Scheme 1c).[16,17] Mechanochemical synthesis can produce mixed-halide perovskites with band gaps tunable over the entire visible spectrum just by varying the halide precursor ratio (Figure 4).[65] As mentioned above, ball milling naturally produces small crystallites. In this case, soluble nanocrystals with narrow photoluminescence with full width at half maximum (FWHM) of ~20 nm and moderate

photoluminescence quantum yields of ~40% were produced by post-synthetic treatment with oleylamine.[65] The relatively lower quantum yields compared to those obtained for colloidal perovskite nanocrystals synthesized by solution-phase methods is believed to be caused by surface trap states and other structural defects induced by ball milling.[50] Nevertheless, quantum yields of up to 80% can be achieved when ball milling is performed in the presence of both oleylamine and oleic acid.[50]

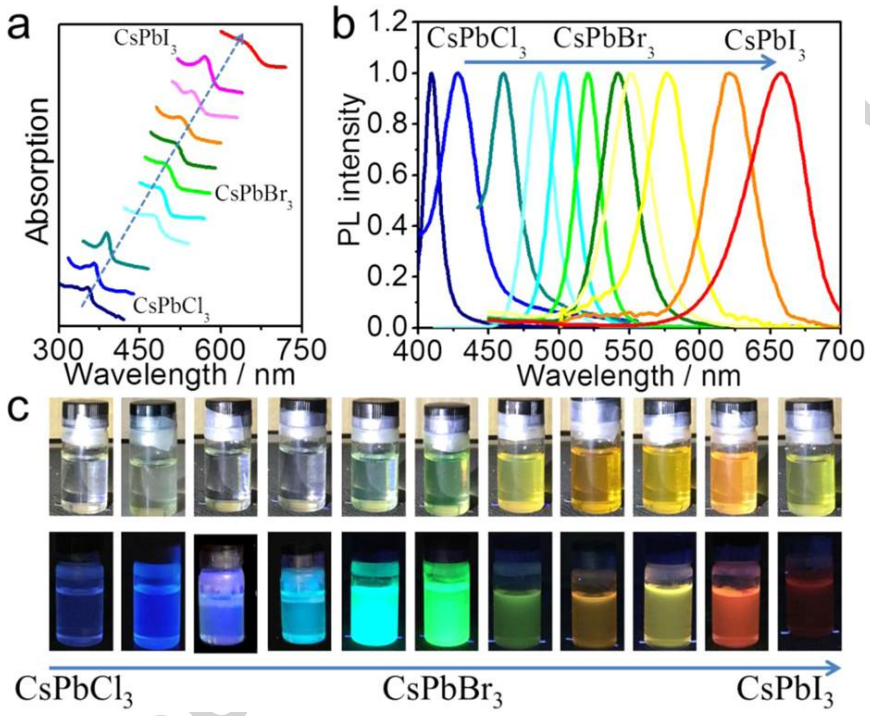

Figure 4. Panchromatic absorption (a) and PL spectra (b), and visual luminescence of mixed-halide $CsPbX_3$ perovskite nanocrystals synthesized by ball milling, post-treated with oleylamine, and suspended in toluene. Reprinted with permission from ref. 65. Copyright 2017 American Chemical Society.

One of the most exciting recent developments in the chemistry of heavily mixed perovskites is the observation of non-stoichiometric phases—and, in some cases, synthesis-specific impurities—by solid-state (ss) NMR, which are silent by the most commonly employed characterization methods, such as optical spectroscopy and XRD. For example, light absorption and XRD would appear to indicate that mixed-halide perovskites are simply made of a single phase. However, ssNMR unambiguously shows that this is not the case. Regardless of the

synthetic method used, ^{207}Pb ssNMR shows mixed-halide perovskites contain a significant amount of non-stoichiometric $[PbX_aX'_{6-a}]^{4-}$ octahedra which are richer in one or another halide, as compared to the XRD-observed phase (Figure 5).[14,15,16,17] Further, ^{207}Pb ssNMR shows that mixed-halide perovskites made by precipitation from solution often contain significant amounts of amorphous XRD-silent impurities, while those made by solvent-free solid-state synthesis methods do not. For example, in the $APb(I,Br)_3$ series, 1:1 precipitation from solution produces a mixture of Br-rich $APbI_aBr_b$ (b >> a) and an uncrystallized form of $APbBr_3$ (A = MA or FA).[14,15,17] Instead, in the absence of solvents, solid-state synthesis of the 1:1 mixed-halide perovskite by either thermal annealing[14,15] or ball milling[16,17] completely eliminates the formation of the uncrystallized single-phase perovskite (Figure 5b *vs.* c). Thus, by eliminating halide-specific solvent-solute interactions,[13] solid-state synthesis methods achieve more uniform halide mixing, and result in mixed-halide perovskites that are significantly higher in purity.[14,15,16,17]

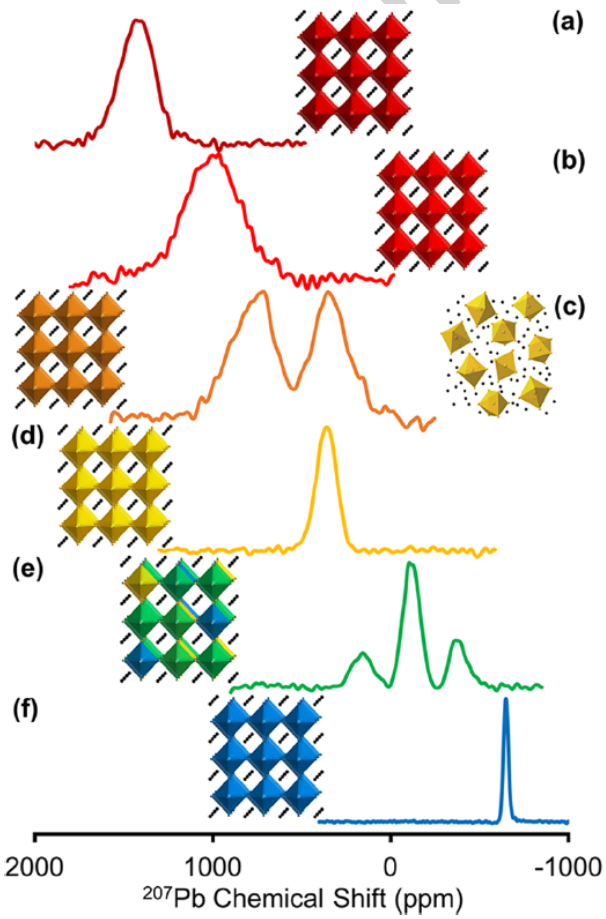

Figure 5. Representative static ^{207}Pb ssNMR spectra of single- and 1:1 mixed-halide $MA(X_{1.5}X'_{1.5})_3$ perovskites. X,X´ = I (a), I,Br from solid-state synthesis (b), I,Br from solution phase synthesis (c), Br (d), Br,Cl (e), Cl (f). Reprinted with permission from ref. 15, https://pubs.acs.org/doi/10.1021/acsenergylett.6b00674. Further permissions related to the material excerpted should be directed to the ACS.

6. Mixed-Cation Halide Perovskites.

The solid-state synthesis of mixed-cation halide perovskites has almost exclusively focused on mechanochemical synthesis of mixed 'A' cation halide perovskites by ball milling AX and BX_2 precursors (Scheme 1b). To simulate film fabrication conditions, this is often followed by thermal annealing between 110–140 °C. A variety of different mixed-cation halide perovskites can be made by this method, including double-,[98,99,100,101,102] triple-,[66,100,102] and quadruple-[100] cation perovskites. Currently, there is only one report of mixed 'B' cation $MASn_{1-x}Pb_xI_3$ perovskites, which can be made from CH_3NH_3I, SnI_2, and PbI_2 precursors by either manual grinding at room temperature or by annealing in a sealed ampule at 200 °C.[40] Mixed $(MA,Cs)PbBr_3$ perovskites can be made by grinding a desired mixture of pre-synthesized $MAPbBr_3$ and $CsPbBr_3$, followed by annealing in an evacuated sealed ampule at 150 °C for 5 days.[72] Solid-state methods are amenable to scale up, enabling the synthesis of gram amounts of mixed-cation halide perovskites that are structurally comparable to thin films made from solution.[100] Interestingly, the use of mechanochemically-prepared mixed-cation halide perovskites as precursors for film deposition can exhibit increased PCE compared to the use of AX and PbX_2 precursors.[98] However, such improvements have been small and limited to lower PCE configurations, and all-time record devices have not yet benefited from mechanochemically prepared precursors. One particularly useful benefit is that mixed-cation halide perovskite powder prepared by ball milling exhibits greater long-term stability as a precursor compared to the storage of AX and PbX_2 precursors in typical DMF/DMSO-based ink.[103] Over time, dimethylammonium formate accumulates in the DMF/DMSO-based ink from the hydrolysis of DMF and affects the perovskite film's stoichiometry, band gap, and structure upon incorporation.[103] Solid-state methods can also be used to incorporate insoluble cation precursors, such as CsCl, which can further improve photovoltaic properties (Figure 6).[66]

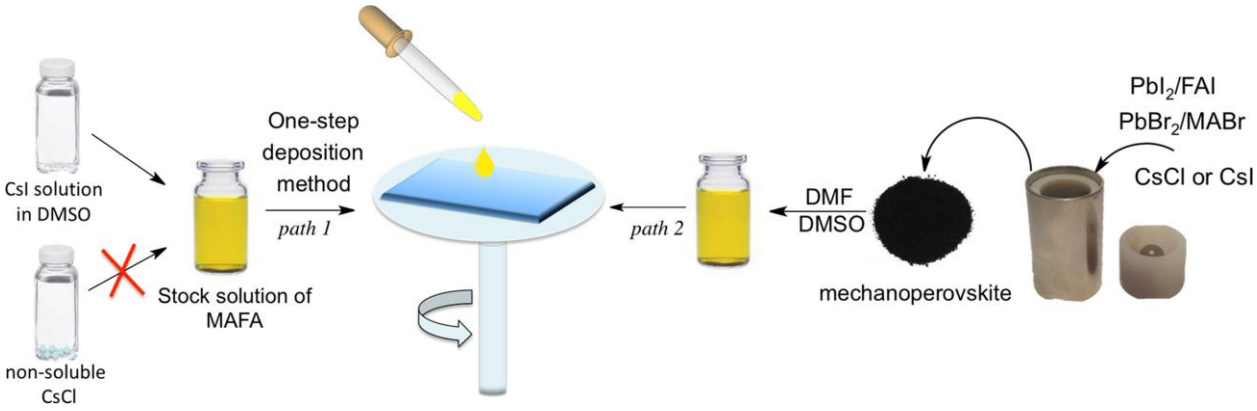

Figure 6. Solar cell ink made from both typical precursors (*path 1*) and mechanochemically-prepared perovskite (*path 2*). Ball milling enables introduction of insoluble precursors into the solar cell ink. Reprinted from ref. 66, Copyright 2018, with permission from Elsevier.

Compared to single-cation halide perovskites, mixed-cation halide perovskites have more tunable band gap and enhanced thermal stability. Further, in the case of Cs- and FA-based mixed-cation halide perovskites, the normally high-temperature 'black' photoactive phase becomes more stable and persists at room temperature. As noted above, the degree of phase segregation and, in this case, the degree of cation incorporation should be taken into account when synthesizing mixed-cation halide perovskites. Incorporating the smaller MA cation into the $FAPbI_3$ lattice readily forms solid solutions of $(MA,FA)PbI_3$, as determined quantitatively by ^{13}C and ^{1}H MAS ssNMR.[99] When $(MA,FA)PbI_3$ is prepared at room temperature by ball milling a mixture of AI and PbI_2 precursors, the photoactive black phase of $FAPbI_3$ forms along the inactive yellow phase at 15% MA loading, and becomes the only phase formed at 25% MA loading.[98] In contrast, a film prepared from solution results in both black and yellow phases at 25% MA, indicating that solid-state methods succeed in affording the black phase at lower MA loading.[98] As shown for mixed-halide systems, mixed-cation halide perovskite films often have a different stoichiometry than their initial precursor mixture.[104] Doping of the GUA cation into both $MAPbI_3$ and $FAPbI_3$ lattices is desirable because of its ability to increase carrier lifetimes and V_{OC} values. Because of its large size, the photoactive black phase of $MAPbI_3$ is only stable up to 40% GUA incorporation, while the photoactive black phase of $FAPbI_3$ is unstable at all GUA incorporation or 'doping' levels.[101] The incorporation of alkali cations (Cs^+, Rb^+, and K^+) into $(MA,FA)PbX_3$ perovskites to form triple and quadruple perovskites was also investigated by ball milling AX and PbX_2 precursors (Scheme 1b). ^{133}Cs, ^{87}Rb, and ^{39}K MAS ssNMR show the

Cs^+ cation is readily incorporated into the perovskite lattice, while incorporation of Rb^+ or K^+ cations is not observed (Figure 7).[100,102] Instead of being incorporated into (MA,FA)PbX_3, Rb^+ and K^+ cations form phase segregated AX domains (A = Rb, K; X = I, Br), along with $APbX_3$ (and $ACsPbX_3$, when Cs^+ is present). [100,102]

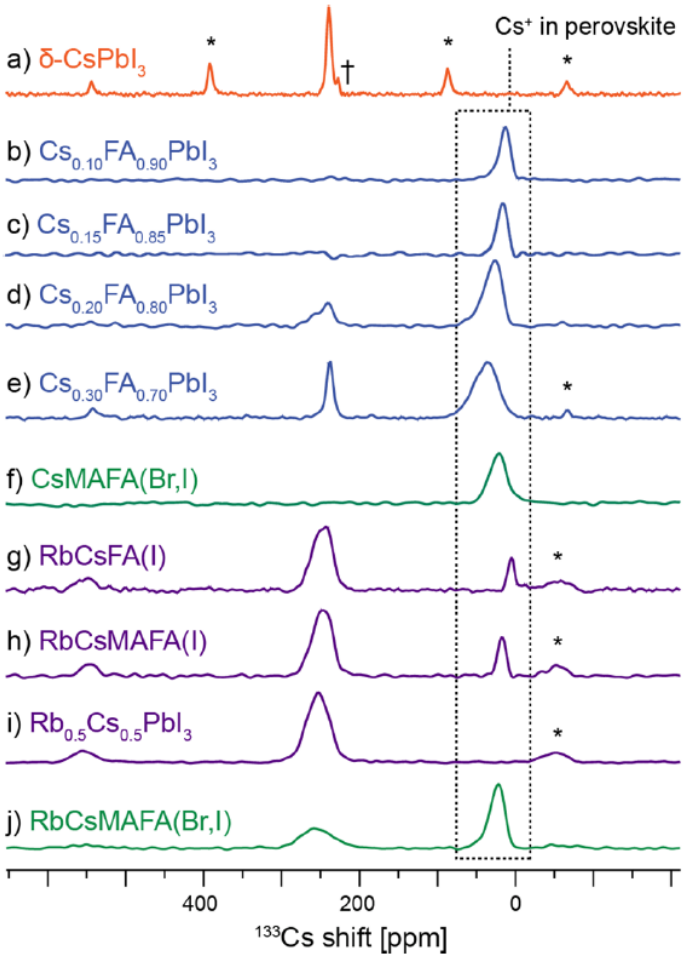

Figure 7. Quantitative ^{133}Cs echo-detected MAS ssNMR spectra of various (Rb,Cs,MA,FA)$Pb(I,Br)_3$ perovskites. Dashed box denotes region where Cs^+ is incorporated. Asterisks (*) indicate spinning sidebands and † is a transmitter artifact. Reprinted with permission from ref. 100, https://pubs.acs.org/doi/10.1021/jacs.7b07223. Further permissions related to the material excerpted should be directed to the ACS.

7. Mixed-Cation–Mixed-Halide Perovskites.

A few reports on the solid-state synthesis of heavily mixed perovskites contain both mixed-cations and mixed-halides. These studies involve ball milling AX and PbX_2 precursors

(Scheme 1b).[66,100,102,103] Mixed-cation and mixed-anion halide perovskites are under intense scrutiny as photovoltaic absorbers. Their many beneficial properties include increased thermal stability and ability to withstand different processing conditions.[8,9,66] The solid-state synthesis of these materials has focused on the preparation of normally hard-to-access precursor inks, for example those containing additives such as CsCl,[66] the preparation of precursor inks with significantly increased shelf stability,[103] and the preparation of large enough samples for phase-segregation studies followed by ssNMR (Figure 7 above).[100,102] These studies show that heavily mixed compositions form readily by solid-state synthesis *via* ball milling. We expect a growing variety of heavily mixed perovskites with both mixed-cations and mixed-anions will become accessible by solvent-free methods.

7. Conclusion.

In summary, halide perovskites can be made by various solid-state methods in the absence of solvents, including ball milling, manual grinding, and thermal annealing. Independence from solvents reduces waste generation, making these methods 'greener,' more industrially relevant, and potentially more scalable. A variety of heavily mixed halide perovskites can be made by solid-state methods, including mixed-halide, mixed-cation, and mixed-halide–mixed-cation perovskites, as well as nanosized perovskites with very bright and narrow photoluminescence emission. Interestingly, mechanochemically prepared mixed-cation halide perovskites are much more stable precursors for inks used in the deposition of solar cells, providing improved photovoltaic performance.

When heavily mixed perovskites are synthesized from solution, each component is subjected to different solute-solvent interactions, often leading to products with unpredictable compositions that do not match the original synthetic loading. In contrast, solvent-free methods circumvent the effects caused by different binding affinities and other solute-solvent interactions. As a result, heavily mixed halide perovskites prepared by solvent-free solid-state methods show much more predictable compositions and significantly suppressed phase segregation, as observed by ssNMR, which has quickly emerged as the tool of choice to truly understand the actual speciation of heavily mixed halide perovskites. These findings show that solid-state methods are superior because they offer higher synthetic control and higher purity in the synthesis of these exciting materials.

In spite of all the benefits of synthesizing halide perovskites by solid-state methods compared to solution methods, solid-state methods are so far incompatible with film fabrication. This limitation is typically overcome by taking a halide perovskite powder, previously prepared by a solid-state method, and dissolving it into an appropriate solvent followed by spin-coating. Improved photovoltaic properties have been reported for films prepared in this way. However, the origin of these improvements is unknown, and solute-solvent interactions can alter the composition of the resulting halide perovskite film. Another promising alternative is melt-processing, which has only been demonstrated for hybrid 2D halide perovskites that exhibit melting points lower than their decomposition temperatures. For melt-processing to be useful beyond hybrid 2D halide perovskites, either the melting point of other halide perovskite compositions must be lowered, or their decomposition temperatures must be increased. Overall, there is a need for developing processes to grow halide perovskite thin films in the solid-state and without the influence of solvents.

Another important question pertains to the actual *in-situ* temperatures produced during mechanochemical synthesis of halide perovskites. To date, a majority of reports on the mechanochemical synthesis of halide perovskites claim that this occurs at room temperature. This is unlikely. When precursors are crushed between metal balls, significant amounts of heat are introduced into the system through mechanical energy. Different groups regularly use different synthetic conditions affecting the total amount of mechanical energy introduced into the system, including the number of different sized balls, rotation speed, and ball-milling time. Thus, ball milling reactions cannot be safely assumed to proceed at room temperature, unless the temperature inside the ball mill is being actively monitored.

Author Information.

Acknowledgements.

J.V. and B.A.R. thank the U.S. National Science Foundation for a CAREER Grant and an AGEP GR Supplement, respectively, from the Division of Chemistry, Macromolecular,

Supramolecular, and Nanochemistry Program (#1253058). We also thank all of our hard-working halide perovskite coworkers—Feng Zhu, Long Men, Himashi Andaraarachchi, Noreen Gentry—and our collaborators and their groups—Aaron Rossini, Sarah Cady, Emily Smith, Jake Petrich, Peter Goodwin, and Jigang Wang.

References.

(1) Green, M. A.; Ho-Bailli, A. Perovskite Solar Cells: The Birth of a New Era in Photovoltaics. *ACS Energy Lett.* **2017**, *2*, 822–830.
(2) National Renewable Energy Laboratory. Best Research-Cell Efficiencies Chart. (Accessed on December 17th, 2018). https://www.nrel.gov/pv/assets/pdfs/pv-efficiency-chart.20181214.pdf.
(3) Wang, K.; Jin, Z.; Liang, L.; Bian, H.; Bai, D.; Wang, H.; Zhang, J.; Wang, Q.; Liu, S. All-Inorganic Cesium Lead Iodide Perovskite Solar Cells with Stabilized Efficiency Beyond 15%. *Nat. Commun.* **2018**, *9*, 4544.
(4) Li, Z.; Klein, T. R.; Kim, D. H.; Yang, M.; Berry, J. J.; van Hest, M. F. A. M.; Zhu, K. Scalable Fabrication of Perovskite Solar Cells. *Nat. Rev. Mater.* **2018**, *3*, 18017.
(5) Sutherland, B. R.; Sargent, E. H. Perovskite Photonic Sources. *Nat. Photon.* **2016**, *10*, 295–302.
(6) Huang, J.; Yuan, Y.; Shao, Y.; Yan, Y. Understanding the Physical Properties of Hybrid Perovskites for Photovoltaic Applications. *Nat. Rev. Mater.* **2017**, *2*, 17042.
(7) Li, W.; Wang, Z.; Deschler, F.; Gao, S.; Friend, R. H.; Cheetham, A. K. Chemically Diverse and Multifunctional Hybrid Organic-Inorganic Perovskites. *Nat. Rev. Mater.* **2017**, *2*, 16099.
(8) Tang, Z.; Uchida, S.; Bessho, T.; Kinoshita, T.; Wang, H.; Awai, F.; Jono, R.; Maitani, M. M.; Nakazaki, J.; Kubo, T.; Segawa, H. Modulations of Various Alkali Metal Cations on Organometal Halide Perovskites and Their influence on Photovoltaic Performance. *Nano Energy* **2018**, *45*, 184–192.
(9) Saliba, M.; Matsui, T.; Seo, J. Y.; Domanski, K.; Correa-Baena, J. P.; Nazeeruddin, M. K.; Zakeeruddin, S. M.; Tress, W.; Abate, A.; Hagfeldt, A.; Grätzel, M. *Energy Environ. Sci.* **2016**, *9*, 1989–1997.
(10) Manser, J. S.; Saidaminov, M. I.; Christians, J. A.; Bakr, O. M.; Kamat, P. V. Making and Breaking of Lead Halide Perovskites. *Acc. Chem. Res.* **2016**, *49*, 330–338.
(11) Zhang, W.; Eperon, G. E.; Snaith, H. J. Metal Halide Perovskites for Energy Applications. *Nat. Energy* **2016**, *1*, 16048.
(12) Bai, S.; Yuan, Z.; Gao, F. Colloidal Metal Halide Perovskite Nanocrystals: Synthesis, Characterization, and Applications. *J. Mater. Chem. C* **2016**, *4*, 3898–3904.
(13) Yoon, S. J.; Stamplecoskie, K. G.; Kamat, P. V. How Lead Halide Complex Chemistry Dictates the Composition of Mixed Halide Perovskites. *J. Phys. Chem. Lett.* **2016**, *7*, 1368–1373.
(14) Rosales, B. A.; Men, L.; Cady, S. D.; Hanrahan, M. P.; Rossini, A. J.; Vela, J. Persistent Dopants and Phase Segregation in Organolead Mixed-Halide Perovskites. *Chem. Mater.* **2016**, *28*, 6848–6859.
(15) Rosales, B. A.; Hanrahan, M. P.; Boote, B. W.; Rossini, A. J.; Smith, E. A.; Vela, J. Lead Halide Perovskites: Challenges and Opportunities in Advanced Synthesis and Spectroscopy. *ACS Energy Lett.* **2017**, *2*, 906–914.

(16) Karmakar, A.; Askar, A. M.; Bernard, G. M.; Terskikh, V. V.; Ha, M.; Patel, S.; Shankar, K.; Michaelis, V. K. Mechanochemical Synthesis of Methylammonium Lead Mixed-Halide Perovskites: Unraveling the Solid-Solution Behavior Using Solid-State NMR. *Chem. Mater.* **2018**, *30*, 2309–2321.
(17) Askar, A. M.; Karmakar, A.; Bernard, G. M.; Ha, M.; Terskikh, V. V.; Wiltshire, B. D.; Patel, S.; Fleet, J.; Shankar, K.; Michaelis, V. K. Composition-Tunable Formamidinium Lead Mixed Halide Perovskites *via* Solvent-Free Mechanochemical Synthesis: Decoding the Pb Environments Using Solid-State NMR Spectroscopy. *J. Phys. Chem. Lett.* **2018**, *9*, 2671–2677.
(18) Brivio, F.; Caetano, C.; Walsh, A. Thermodynamic Origin of Photoinstability in the $CH_3NH_3Pb(I_{1-x}Br_x)_3$ Hybrid Halide Perovskite Alloy. *J. Phys. Chem. Lett.* **2016**, *7*, 1083–1087.
(19) Hanrahan, M. P.; Men, L.; Rosales, B. A.; Vela, J.; Rossini, A. J. Sensitivity-Enhanced ^{207}Pb Solid-State NMR Spectroscopy for the Rapid, Non-Destructive Characterization of Organolead Halide Perovskites. *Chem. Mater.* **2018**, *30*, 7005–7015.
(20) Men, L.; White, M. A.; Andaraarachchi, H.; Rosales, B. A.; Vela, J. Synthetic Development of Low Dimensional Materials. *Chem. Mater.* **2017**, *29*, 168–175.
(21) Baláž, P.; Achimovičová, M.; Baláž, M.; Billik, P.; Cherkezova-Zheleva, Z.; Criado, J. M.; Delogu, F.; Dutková, E.; Gaffet, E.; Gotor, F. J.; Kumar, R.; Mitov, I.; Rojac, T.; Senna, M.; Streletskii, A.; Wieczorek- Ciurowa, K. Hallmarks of Mechanochemistry: From Nanoparticles to Technology. *Chem. Soc. Rev.* **2013**, *42*, 7571–7637.
(22) Chroneos, A.; Vovk, R. V.; Goulatis, I. L.; Goulatis, L.; I. Oxygen Transport in Perovskite and Related Oxides: A Brief Review. *J. Alloys Compd.* **2010**, *494*, 190–195.
(23) Stølen, S.; Bakken, E.; Mohn, C. E. Oxygen-Deficient Perovskites: Linking Structure, Energetics and Ion Transport. *Phys. Chem. Chem. Phys.* **2006**, *8*, 429–447.
(24) Ma, H. H.; Imran, M.; Dang, Z.; Hu, Z. Growth of Metal Halide Perovskite, From Nanocrystal to Micron-Scale Crystal: A Review. *Crystals* **2018**, *8*, 182.
(25) Vicente, N.; Garcia-Belmonte, G. Organohalide Perovskites are Fast Ionic Conductors. *Adv. Energy Mater.* **2017**, *7*, 1700710.
(26) Walsh, A.; Stranks, S. D. Taking Control of Ion Transport in Halide Perovskite Solar Cells. *ACS Energy Lett.* **2018**, *3*, 1983–1990.
(27) Yuan, Y.; Huang, J. Ion Migration in Organometal Trihalide Perovskite and Its Impact on Photovoltaic Efficiency and Stability. *Acc. Chem. Res.* **2016**, *49*, 286–293.
(28) Frost, J. M.; Walsh, A. What is Moving in Hybrid Halide Perovskite Solar Cells? *Acc. Chem. Res.* **2016**, *49*, 528–535.
(29) Mosconi, E.; De Angelis, F. Mobile Ions in Organohalide Perovskites: Interplay of Electronic Structure and Dynamics. *ACS Energy Lett.* **2016**, *1*, 182–188.
(30) Senocrate, A.; Moudrakovski, I.; Acartürk, T.; Merkle, R.; Kim, G. Y.; Starke, U.; Grätzel, M.; Maier, J. Slow $CH_3NH_3^+$ Diffusion in $CH_3NH_3PbI_3$ Under Light Measured by Solid-State NMR and Tracer Diffusion. *J. Phys. Chem. C* **2018**, *122*, 21803–21806.
(31) Rehman, W.; McMeekin, D. P.; Patel, J. B.; Milot, R. L.; Johnston, M. B.; Snaith, H. J.; Herz, L. M. Photovoltaic Mixed-Cation Lead Mixed-Halide Perovskites: Links Between Crystallinity, Photo-Stability and Electronic Properties. *Energy Environ. Sci.* **2017**, *10*, 361–369.
(32) McMeekin, D. P.; Sadoughi, G.; Rehman, W.; Eperon, G. E.; Saliba, M.; Hörantner, M. T.; Haghighirad, A.; Sakai, N.; Korte, L.; Rech, B.; Johnston, M. B.; Herz, L. M.; Snaith, H. J. A Mixed-Cation Lead Mixed-Halide Perovskite Absorber for Tandem Solar Cells. *Science* **2016**, *351*, 6269, 151–155.

(33) Zheng, C.; Rubel, O. Ionization Energy as a Stability Criterion for Halide Perovskites. *J. Phys. Chem. C* **2017**, *121*, 11977–11984.
(34) Mizusaki, J.; Arai, K.; Fueki, K. Ionic Conduction of the Perovskite-Type Halides. *Solid State Ionics* **1983**, *11*, 203–211.
(35) Zhang, M.; Zheng, Z.; Fu, Q.; Chen, Z.; He, J.; Zhang, S.; Yan, L.; Hu, Y.; Luo, W. Growth and Characterization of All-Inorganic Lead Halide Perovskite Semiconductor $CsPbBr_3$ Single Crystals. *CrystEngComm* **2017**, *19*, 6797–6803.
(36) Stoumpos, C. C.; Malliakas, C. D.; Peters, J. A.; Liu, Z.; Sebastian, M.; Im, J.; Chasapis, T. C.; Wibowo, A. C.; Chung, D. Y.; Freeman, A. J.; Wessels, B. W.; Kanatzidis, M. G. *Cryst. Growth Des.* **2013**, *13*, 2722–2727.
(37) Fayon, F.; Vaills, Y.; Simon, P.; Echegut, P.; Bessada, C.; Emery, J.; Buzare, J.-Y. Study of $CsPbCl_3$ Between T = 47 °C and the Melting Point by the ^{133}Cs NMR and Gd^{3+} EPR Measurements. *Ferroelectrics* **1996**, *185*, 201–204.
(38) Chung, I.; Song, J.-H.; Im, J.; Androulakis, J.; Malliakas, C. D.; Li, H.; Freeman, A. J.; Kenney, J. T.; Kanatzidis, M. G. $CsSnI_3$: Semiconductor or Metal? High Electrical Conductivity and Strong Near-Infrared Photoluminescence from a Single Material. High Hole Mobility and Phase-Transitions. *J. Am. Chem. Soc.* **2012**, *134*, 8579–8587.
(39) Peedikakkandy, L.; Bhargava, P. Composition Dependent Optical, Structural, and Photoluminescence Characteristics of Cesium Tin Halide Perovskites. *RSC Adv.* **2016**, *6*, 19857–19860.
(40) Stoumpos, C. C.; Malliakas, C. D.; Kanatzidis, M. G. Semiconducting Tin and Lead Iodide Perovskites with Organic Cations: Phase Transitions, High Mobilities, and Near-Infrared Photoluminescent Properties. *Inorg. Chem.* **2013**, *52*, 9019–9038.
(41) Dualeh, A.; Gao, P.; Seok, S. I.; Nazeeruddin, M. K.; Grätzel, M. Thermal Behavior of Methylammonium Lead-Trihalide Perovskite Photovoltaic Light Harvesters. *Chem. Mater.* **2014**, *26*, 6160–6164.
(42) Liu, Y.; Yang, Z.; Cui, D.; Ren, X.; Sun, J.; Liu, X.; Zhang, J.; Wei, Q.; Fan, H.; Yu, F.; Zhang, X.; Zhao, C.; Liu, S. Two-Inch-Sized Perovskite $CH_3NH_3PbX_3$ (X = Cl, Br, I) Crystals: Growth and Characterization. *Adv. Mater.* **2015**, *27*, 5176–5183.
(43) Ju, D.; Dang, Y.; Zhu, Z.; Liu, H.; Chueh, C.-C.; Li, X.; Wang, L.; Hu, X.; Jen, A. K.-Y.; Tao, X. Tunable Band Gap and Long Carrier Recombination Lifetime of Stable Mixed $CH_3NH_3Pb_xSn_{1-x}Br_3$ Single Crystals. *Chem. Mater.* **2018**, *30*, 1556–1565.
(44) Pang, S.; Hu, H.; Zhang, J.; Lv, S.; Yu, Y.; Wei, F.; Qin, T.; Xu, H.; Liu, Z.; Cui, G. $NH_2CH{=}NH_2PbI_3$: An Alternative Organolead Iodide Perovskite Sensitizer for Mesoscopic Solar Cells. *Chem. Mater.* **2014**, *26*, 1485–1491.
(45) Han, Q.; Bae, S.-H.; Sun, P.; Hsieh, Y.-T.; Yang, Y.; Rim, Y. S.; Zhao, H.; Chen, Q.; Shi, W.; Li, G.; Yang, Y. Single Crystal Formamidinium Lead Iodide ($FAPbI_3$): Insight into the Structural, Optical, and Electrical Properties. *Adv. Mater.* **2016**, *28*, 2253–2258.
(46) Hanusch, F. C.; Wiesenmayer, E.; Mandel, E.; Binek, A.; Angloher, P.; Fraunhofer, C.; Giesbrecht, N.; Feckl, J. M.; Jaegermann, W.; Johrendt, D.; Bein, T.; Docampo, P. Efficient Planar Heterojunction Perovskite Solar Cells Based on Formamidinium Lead Bromide. *J. Phys. Chem. Lett.* **2014**, *5*, 2791–2795.
(47) Juarez-Perez, E. J.; Hawash, Z.; Raga, S. R.; Ono, L. K.; Qi, Y. Thermal Degradation of $CH_3NH_3PbI_3$ Perovskite into NH_3 and CH_3I Gases Observed by Coupled Thermogravimetry-Mass Spectrometry Analysis. *Energy Environ. Sci.* **2016**, *9*, 3406–3410.

(48) Takacs, L. The Historical Development of Mechanochemistry. *Chem. Soc. Rev.* **2013**, *42*, 7649–7659.
(49) Gutman, E. M. *Mechanochemistry of Materials*; Cambridge International Science Publishing: Cambridge, 1998;
(50) Protesescu, L.; Yakunin, S.; Nazarenko, O.; Dirin, D. N.; Kovalenko, M. V. Low-Cost Synthesis of Highly Luminescent Colloidal Lead Halide Perovskite Nanocrystals by Wet Ball Milling. *ACS Appl. Nano Mater.* **2018**, *1*, 1300–1308.
(51) Berhe, T. A.; Su, W.-N.; Chen, C.-H.; Pan, C.-J.; Cheng, J.-H.; Chen, H.-M.; Tsai, M.-C.; Chen, L.-Y.; Dubale, A. A.; Hwang, B.-J. Organometal Halide Perovskite Solar Cells: Degradation and Stability. *Energy Environ. Sci.* **2016**, *9*, 323–356.
(52) Prochowicz, D.; Franckevičius, M.; Cieślak, A. M.; Zakeeruddin, S. M.; Grätzel, M.; Lewiński, J. Mechanosynthesis of the Hybrid Perovskite $CH_3NH_3PbI_3$: Characterization and the Corresponding Solar Cell Efficiency. *J. Mater. Chem. A* **2015**, *3*, 20772–20777.
(53) Manukyan, K. V.; Yeghishyan, A. V.; Moskovskikh, D. O.; Kapaldo, J.; Mintairov, A.; Mukasyan, A. S. Mechanochemical Synthesis of Methylammonium Lead Iodide Perovskite. *J Mater. Sci*. **2016**, *51*, 9123–9130.
(54) Prochowicz, D.; Yadav, P.; Saliba, M.; Saski, M.; Zakeeruddin, S. M.; Lewiński, J.; Grätzel, M. Reduction in the Interfacial Trap Density of Mechanochemically Synthesized $MAPbI_3$. *ACS Appl. Mater. Interfaces*, **2017**, *9*, 28418–28425.
(55) Posudievsky, O. Y.; Konoshchuk, N. V.; Karbivskyy, V. L.; Boiko, O. P.; Koshechko, V. G.; Pokhodenko, V. D. Structural and Spectral Characteristics of Mechanochemically Prepared $CsPbBr_3$. *Theor. Exp. Chem*. **2017**, *53*, 235–243.
(56) Dhar, J.; Sil, S.; Hoque, N. A.; Dey, A.; Das, S.; Ray, P. P.; Sanyal, D. Lattice-Defect-Induced Piezo Response in Methylammonium-Lead-Iodide Perovskite Based Nanogenerator. *ChemistrySelect* **2018**, *3*, 5304–5312.
(57) Jana, A.; Mittal, M.; Singla, A.; Sapra, S. Solvent-Free, Mechanochemical Syntheses of Bulk Trihalide Perovskites and their Nanoparticles. *Chem. Commun.* **2017**, *53*, 3046–3049.
(58) Posudievsky, O. Y.; Konoshchuk, N. V.; Shkavro, A. G.; Karbivskiy, V.; Koshechko, V. G.; Pokhodenko, V. D. Nanostructured Mechanochemically Prepared Hybrid Perovskites Based on PbI_2 and Alkylammonium Halides for Optoelectronic Applications. *ACS Appl. Nano Mater*. **2018**, *1*, 4145–4155..
(59) Pal, P.; Saha, S.; Banik, A.; Sarkar, A.; Biswas, K. All-Solid-State Mechanochemical Synthesis and Post-Synthetic Transformation of Inorganic Perovskite-Type Halides. *Chem. Eur. J.* **2018**, *24*, 1811–1815.
(60) Li, J.; Stoumpos, C. C.;Trimarchi, G. G.; Chung, I.; Mao, L.; Chen, M.; Wasielewski, M. R.; Wang, L.; Kanatzidis, M. G. Air-Stable Direct Bandgap Perovskite Semiconductors: All-Inorganic Tin-Based Heteroleptic Halides AxSnClyIz (A = Cs, Rb). *Chem. Mater.* **2018**, *30*, 4847–4856.
(61) Jodlowski, A. D.; Yépez, A.; Luque, R.; Camacho, L.; de Miguel, G. Benign-by-Design Solventless Mechanochemical Synthesis of Three-, Two-, and One-Dimensional Hybrid Perovskites. *Angew. Chem. Int. Ed*. **2016**, *55*, 14972–14977.
(62) Papavassiliou, G. C.; Vidali, M.-S.; Pagona, G.; Mousdis, G. A.; Karousis, N.; Koutselas, I. Effects of Organic Moieties on the Photoluminescence Spectra of Perovskite-Type Tin Bromide Based Compounds. *J. Phys. Chem. Solids* **2015**, *79*, 1–6.

(63) Singhal, N.; Chakraborty, R.; Ghosh, P.; Nag, A. Low-Bandgap $Cs_4CuSb_2Cl_{12}$ Layered Double Perovskite: Synthesis, Reversible Thermal Changes, and Magnetic Interaction. *Chem. Asian J.* **2018**, *13*, 2085–2092.
(64) Elseman, A. M.; Rashad, M. M.; Hassan, A. M.; Easily Attainable, Efficient Solar Cell with Mass Yield of Nanorod Single-Crystalline Organo-Metal Halide Perovskite Based on a Ball Milling Technique. *ACS Sustainable Chem. Eng.* **2016**, *4*, 4875–4886.
(65) Zhu, Z.-Y.; Yang, Q.-Q.; Gao, L.-F.; Zhang, L.; Shi, A.-Y.; Sun, C.-L.; Wang, Q.; Zhang, H.-L.; Solvent-Free Mechanosynthesis of Composition-Tunable Cesium Lead Halide Perovskite Quantum Dots. *J. Phys. Chem. Lett.* **2017**, *8*, 1610–1614.
(66) Prochowicz, D.; Yadav, P.; Saliba, M.; Kubicki, D. J.; Tavakoli, M. M.; Zakeeruddin, S. M.; Lewiński, J.; Emsley, L.; Grätzel, M. One-Step Mechanochemical Incorporation of an Insoluble Cesium Additive for High Performance Planar Heterojunction Solar Cells. *Nano Energy* **2018**, *49*, 523–528.
(67) Smart, L. E.; Moore, E. A. Synthesis of Solids. *Solid State Chemistry: An Introduction*, 4th Ed.; CRC Press: Boca Raton, 2012;
(68) Scaife, D. E.; Weller, P. F.; Fisher, W. G. Crystal Preparation and Properties of Cesium Tin(II) Trihalides. *J. Solid State Chem.* **1974**, *9*, 308–314.
(69) Shum, K.; Chen, Z.; Qureshi, J.; Yu, C.; Wang, J. J.; Pfenninger, W.; Vockic, N.; Midgley, J.; Kenney, J. T. Synthesis and Characterization of $CsSnI_3$ Films. *Appl. Phys. Lett.* **2010**, *96*, 221903.
(70) Chung, I.; Lee, B.; He, J.; Chang, R. P. H.; Kanatzidis, M. G. All-Solid-State Dye-Sensitized Solar Cells with High Efficiency. *Nature* **2012**, *485*, 486–489.
(71) Kontos, A. G.; Kaltzoglou, A.; Siranidi, E.; Palles, D.; Angeli, G. K.; Arfanis, M. K.; Psycharis, V.; Raptis, Y. S.; Kamitsos, E. I.; Trikalitis, P. N.; Stoumpos, C. C.; Kanatzidis, M. G.; Falaras, P. Structural Stability, Vibrational Properties, and Photoluminescence in $CsSnI_3$ Perovskite Upon the Addition of SnF_2. *Inorg. Chem.* **2017**, *56*, 84–91.
(72) Mozur, E. M.; Maughan, A. E.; Cheng, Y.; Huq, A.; Jalarvo, N.; Daemen, L. L.; Neilson, J. R. Orientational Glass Formation in Substituted Hybrid Perovskites. *Chem. Mater*. **2017**, *29*, 10168–10177.
(73) Mao, L.; Stoumpos, C. C.; Kanatzidis, M. G. Two-Dimensional Hybrid Halide Perovskites: Principles and Promises. *J. Am. Chem. Soc. ASAP*, DOI: 10.1021/jacs.8b10851.
(74) Mao, L.; Wu, Y.; Stoumpos, C. C.; Traore, B.; Katan, C.; Even, J.; Wasielewski, M. R.; Kanatzidis, M. G. Tunable White-Light Emission in Single-Cation-Templated Three-Layered 2D Perovskites $(CH_3CH_2NH_3)_4Pb_3Br_{10-x}Cl_x$. *J. Am. Chem. Soc.* **2017**, *139*, 11956–11963.
(75) Papavassiliou G.C., Koutselas I.B., Mousdis G.A., Papaioannou G.J. Some Organic-Inorganic Hybrid Semiconductors Obtained from Melts. In *Molecular Low Dimensional and Nanostructured Materials for Advanced Applications*; Graja, A., Bułka, B.R., Kajzar, F., Eds.; Springer: Dordrecht, 2002; Vol. 59, pp 319–322.
(76) Li, J.; Yu, Q.; He, Y.; Stoumpos, C. C.; Niu, G.; Trimarchi, G. G.; Guo, H.; Dong, G.; Wang, D.; Wang, L.; Kanatzidis, M. G. $Cs_2PbI_2Cl_2$, All-Inorganic Two-Dimensional Ruddlesden-Popper Mixed Halide Perovskite with Optoelectronic Response. *J. Am. Chem. Soc.* **2018**, *140*, 11085–11090.
(77) Mitzi, D. B.; Liang, K. Preparation and Properties of $(C_4H_9NH_3)_2EuI_4$: A Luminescent Organic-Inorganic Perovskite with a Divalent Rare-Earth Metal Halide Framework. *Chem. Mater.* **1997**, *9*, 2990–2995.

(78) Li, Y.-J.; Wu, T.; Sun, L.; Yang, R.-X.; Jiang, L.; Cheng, P.-F.; Hao, Q.-Q.; Wang, T.-J.; Lu, R.-F.; Deng, W.-Q. Lead-Free and Stable Antimony-Silver-Halide Double Perovskite $(CH_3NH_3)_2AgSbI_6$. *RSC Adv.* **2017**, *7*, 35175–3180.
(79) Hutter, E. M.; Gélvez-Rueda, M. C.; Bartesaghi, D.; Grozema, F. C.; Savenije, T. J. Band-Like Charge Transport in $Cs_2AgBiBr_6$ and Mixed Antimony-Bismuth $Cs_2AgBi_{1-x}Sb_xBr_6$ Halide Double Perovskites. *ACS Omega* **2018**, *3*, 11655–11662.
(80) Du, K.-Z.; Meng, W.; Wang, X.; Yan, Y.; Mitzi, D. B. Bandgap Engineering of Lead-Free Double Perovskite $Cs_2AgBiBr_6$ Through Trivalent Metal Alloying. *Angew. Chem. Int. Ed.* **2017**, *56*, 8158–8162.
(81) McClure, E. T.; Ball, M. R.; Windl, W.; Woodward, P. M. Cs_2AgBiX_6 (X = Br, Cl): New Visible Light Absorbing, Lead-Free Halide Perovskite Semiconductors. *Chem. Mater.* **2016**, *28*, 1348–1354.
(82) Filip, M. R.; Hillman, S.; Haghighirad, A. A.; Snaith, H. J.; Giustino, F. Band Gaps of the Lead-Free Halide Double Perovskites $Cs_2BiAgCl_6$ and $Cs_2BiAgBr_6$ from Theory and Experiment. *J. Phys. Chem. Lett.* **2016**, *7*, 2579–2585.
(83) Sun, Q.; Xu, Y.; Zhang, H.; Xiao, B.; Liu, X.; Dong, J.; Cheng, Y.; Zhang, B.; Jie, W. Kanatzidis, M. G. Optical and Electronic Anisotropies in Perovskitoid Crystals of $Cs_3Bi_2I_9$ Studies of Nuclear Radiation Detection. *J. Mater. Chem. A* **2018**, *6*, 23388–23395.
(84) Sidey, V. I.; Voroshilov, Y. V.; Kun, S.V.; Peresh, E. Y. Crystal Growth and X-Ray Structure Determination of $Rb_3Bi_2I_9$. *J. Alloys Compd.* **2000**, *296*, 53–58.
(85) McCall, K. M.; Liu, Z.; Trimarchi, G.; Stoumpos, C. C.; Lin, W.; He, Y.; Hadar, I.; Kanatzidis, M. G.; Wessels, B. W. α-Particle Detection and Charge Transport Characteristics in the $A_3M_2I_9$ Defect Perovskites (A = Cs, Rb; M = Bi, Sb). *ACS Photonics* **2018**, *5*, 3748–3762.
(86) McCall, K. M.; Stoumpos, C. C.; Kostina, S. S.; Kanatzidis, M. G.; Wessels, B. W. Strong Electron-Phonon Coupling and Self-Trapped Excitons in the Defect Halide Perovskites $A_3M_2I_9$ (A = Cs, Rb; M = Bi, Sb). *Chem. Mater.* **2017**, *29*, 4129–4145.
(87) Wosylus, A.; Schwarz, U.; Ruck, M. Die Kristallstruktur von $Tl_3Bi_2I_9$: Eine Komplexe Ausdünnungs- und Verzerrungsvariante des Perowskit-Typs. *Z. Anorg. Allg. Chem.* **2005**, *631*, 1055–1059.
(88) Li, T.; Dunlap-Shohl, W. A.; Reinheimer, E. W.; Le Magueres, P.; Mitzi, D. B. Melting Temperature Suppression of Layered Hybrid Lead Halide Perovskites *Via* Organic Ammonium Branching. *Chem. Sci. Advanced Article*, DOI: 10.1039/c8sc03863e.
(89) Li, T.; Dunlap-Shohl, W. A.; Han, Q.; Mitzi, D. B. Melt Processing of Hybrid Organic-Inorganic Lead Iodide Layered Perovskites. *Chem. Mater.* **2017**, *29*, 6200–6204.
(90) Mitzi, D. B.; Medeiros, D. R.; DeHaven, P. W. Low-Temperature Melt Processing of Organic-Inorganic Hybrid Films. *Chem. Mater.* **2002**, *14*, 2839–2841.
(91) Mitzi, D. B.; Dimitrakopoulos, C. D.; Rosner, J.; Medeiros, D. R.; Xu, Z.; Noyan, C.; Hybrid Field-Effect Transistor Based on a Low-Temperature Melt-Processed Channel Layer. *Adv. Mater.* **2002**, *14*, 1772–1776.
(92) Nejand, B. A.; Gharibzadeh, S.; Ahmadi, V.; Shahverdi, H. R. Novel Solvent-free Perovskite Deposition in Fabrication of Normal and Inverted Architectures of Perovskite Solar Cells. *Sci. Rep.* **2016**, *6*, 33649.
(93) Dunlap-Shohl, W. A.; Zhou, Y.; Padture, N. P.; Mitzi, D. B. Synthetic Approaches for Halide Perovskite Thin Films. *Chem. Rev. ASAP*, DOI: 10.1021/acs.chemrev.8b00318.

(94) Du, K.-Z.; Wang, X.; Han, Q.; Yan, Y.; Mitzi, D. B. Heterovalent B-Site Co-Alloying Approach for Halide Perovskite Bandgap Engineering. *ACS Energy Lett.* **2017**, *2*, 2486–2490.
(95) Guhrenz, C.; Benad, A.; Ziegler, C.; Haubold, D.; Gaponik, N.; Erychmüller, A. Solid-State Anion Exchange Reactions for Color Tuning of $CsPbX_3$ Perovskite Nanocrystals. *Chem. Mater*. **2016**, *28*, 9033–9040.
(96) Pan, D.; Fu, Y.; Chen, J.; Czech, K. J.; Wright, J. C. Jin, S. Visualization and Studies of Ion-Diffusion Kinetics in Cesium Lead Bromide Perovskite Nanowires. *Nano Lett.* **2018**, *18*, 1807–1813.
(97) Sadhukhan, P.; Kundu, S.; Roy, A.; Ray, A.; Maji, P.; Dutta, H.; Pradhan, S. K.; Das, S. Solvent-Free Solid-State Synthesis of High Yield Mixed Halide Perovskites for Easily Tunable Composition and Band Gap. *Cryst. Growth Des.* **2018**, *18*, 3428–3432.
(98) Prochowicz, D.; Yadav, P.; Saliba, M.; Saski, M.; Zakeeruddin, S. M.; Lewiński, J.; Grätzel, M. Mechanosynthesis of Pure Phase Mixed-Cation $MA_xFA_{1-x}PbI_3$ Hybrid Perovskites: Photovoltaic Performance and Electrochemical Properties. *Sustainable Energy Fuels* **2017**, *1*, 689–693.
(99) Kubicki, D. J.; Prochowicz, D.; Hofstetter, A.; Péchy, P.; Zakeeruddin, S. M.; Grätzel, M.; Emsley, L. Cation Dynamics in Mixed-Cation $(MA)_x(FA)_{1-x}PbI_3$ Hybrid Perovskites from Solid-State NMR. *J. Am. Chem. Soc.* **2017**, *139*, 10055–10061.
(100) Kubicki, D.; Prochowicz, D.; Hofstetter, A.; Zakeeruddin, S. M.; Grätzel, M.; Emsley, L. Phase Segregation in Cs-, Rb- and K-Doped Mixed-Cation $(MA)_x(FA)_{1-x}PbI_3$ Hybrid Perovskites from Solid-State NMR. *J. Am. Chem. Soc.* **2017**, *139*, 14173–14180.
(101) Kubicki, D. J.; Prochowicz, D.; Hofstetter, A.; Saski, M.; Yadav, P.; Bi, D.; Pellet, N.; Lewiński, J.; Zakeeruddin, S. M.; Grätzel, M.; Emsley, L. Formation of Stable Mixed Guanidinium-Methylammonium Phases with Exceptionally Long Carrier Lifetimes for High-Efficiency Lead Iodide-Based Perovskite Photovoltaics. *J. Am. Chem. Soc.* **2018**, *140*, 3345–3351.
(102) Kubicki, D. J.; Prochowicz, D.; Hofstetter, A.; Zakeeruddin, S. M.; Grätzel, M.; Emsley, L. Phase Segregation in Potassium-Doped Lead Halide Perovskites from ^{39}K Solid-State NMR at 21.1 T. *J. Am. Chem. Soc.* **2018**, *140*, 7232–7238.
(103) Dou, B.; Wheeler, L. M.; Christians, J. A.; Moore, D. T.; Harvey, S. P.; Berry, J. J.; Barnes, F. S.; Shaheen, S. E.; van Hest, M. F. A. M. Degradation of Highly Alloyed Metal Halide Perovskite Precursor Inks: Mechanism and Storage Solutions. *ACS Energy Lett.* **2018**, *3*, 979–985.
(104) Pareja-Rivera, C.; Solís-Cambero, A. L.; Sánchez-Torres, M.; Lima, E.; Solis-Ibarra, D. On the True Composition of Mixed-Cation Perovskite Films. *ACS Energy Lett.* **2018**, *3*, 2366–2367.

Highlights

- Many of the best performing halide perovskite solar cells are made of materials containing a mixture of various organic and inorganic ions.
- The formation of halide perovskites in the solid-state proceeds by vacancy- and interstitial-diffusion mechanisms.

- Ball milling, manual grinding, and thermal annealing are the most common methods used to synthesize halide perovskites in the solid-state; ball milling results in small particle sizes, while thermal annealing results in large particle sizes.
- Solvent-free solid-state methods are superior to solution-phase methods because they enable more controllable synthesis of mixed perovskites with enhanced purity.
- Solid-state nuclear magnetic resonance is the method of choice to determine the presence of amorphous impurities and phase segregation in mixed perovskites.